

# Hydration and Temperature Dependence of $^{13}\text{C}$ and $^1\text{H}$ NMR Spectra of the DMPC Phospholipid Membrane and Complete Resonance Assignment of Its Crystalline State

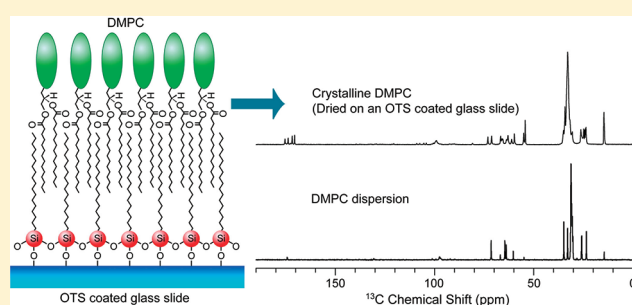
Kaoru Nomura,<sup>\*,†</sup> Masami Lintuluoto,<sup>‡</sup> and Kenichi Morigaki<sup>§</sup>

<sup>†</sup>Suntory Foundation for Life Sciences, Bioorganic Research Institute, 1-1-1 Wakayamadai, Shimamoto-Cho, Mishima-Gun, Osaka 618-8503, Japan

<sup>‡</sup>Faculty of Life and Environmental Sciences Department of Environmental Information, Kyoto Prefectural University, Shimogamo-Hanki-cho, Sakyou, Kyoto, 606-8522, Japan

<sup>§</sup>Research Center for Environmental Genomics, Kobe University, 1-1 Rokkodai, Nada-ku, Kobe, 657-8501, Japan

**ABSTRACT:** Inhomogeneous line broadening due to conformational distributions of molecules is one of the troublesome problems in solid-state NMR spectroscopy. The best possible way to avoid it is to crystallize the sample. Here, we present a highly resolved  $^{13}\text{C}$  cross-polarization (CP) magic angle spinning (MAS) NMR spectrum of the highly ordered crystalline 1,2-dimyristoyl-*sn*-glycero-3-phosphocholine (DMPC) and completely assigned it using two-dimensional (2D) solid-state NMR spectra, dipolar heteronuclear correlation (HETCOR) spectra, scalar heteronuclear J coupling based chemical shift correlation (MAS-J-HMQC) spectra, and Dipolar Assisted Rotational Resonance (DARR) spectra. A comparison between assigned chemical shift values by solid-state NMR in this study and the calculated chemical shift values for X-ray crystal DMPC structures shows good agreement, indicating that the two isomers in the crystalline DMPC take the same conformation as the X-ray crystal structure. The phase diagram of the low hydration level of DMPC ( $3 \leq n_w \leq 12$ ) determined by  $^1\text{H}$  and  $^{13}\text{C}$  NMR spectra indicates that DMPC takes a crystalline state only in a very narrow region around  $n_w = 4$  and  $T < 313$  K. These findings provide us with conformational information on crystalline DMPC and the physical properties of DMPC at a low hydration level and can possibly help us obtain a highly resolved solid-state NMR spectrum of microcrystalline membrane-associated protein samples.



## 1. INTRODUCTION

Solid-state NMR spectroscopy is one of the most effective methods to obtain structural and dynamic information on membrane-associated molecules. For such samples, many kinds of techniques using solid-state NMR have been developed under magic angle spinning (MAS) or static conditions. MAS allows us to investigate highly resolved NMR spectra by eliminating spectral broadening arising from anisotropic interactions, like dipolar and anisotropic chemical shift (CSA) interactions.<sup>1,2</sup> Elimination of line broadening can be achieved by rotating a sample about an axis which is tilted by angle  $\theta$  ( $\theta = 54.7^\circ$ ) with respect to a static field. Under this condition, the special terms ( $3 \cos^2 \theta - 1$ ) in such anisotropic interactions are averaged to be zero. Thus, only isotropic chemical shift values remain. Then, we can also obtain molecular topological information by selectively recoupling for specific anisotropic interaction at the specific time, based on the fact that the interaction possesses internuclear distance and dihedral angle information.

However, since such anisotropic interactions are scaled down due to rapid molecular motion in fully hydrated membrane samples,<sup>3</sup> collecting important information on internuclear

distance and dihedral angles in such samples is often difficult. Molecular mobility could be reduced if we dry the sample, but in lyophilized samples, molecules might possess conformational heterogeneity, which results in broadening the line width of the NMR spectrum.<sup>4</sup> Since line broadening resulting from molecular conformational heterogeneity is caused by distribution of the averaged isotropic shift values, this difficulty cannot be removed under MAS. The best possible way to eliminate the conformational distribution is to order the molecules.

For soluble globular proteins, microcrystalline samples have been used to obtain high-resolution solid-state NMR spectra under MAS without line broadening resulting from conformational heterogeneity.<sup>5–8</sup> Sub-parts per million resolution signals have been available in such samples with the use of high-field instruments. A solid-state NMR approach for microcrystalline protein is useful when X-ray diffraction is not available due to insufficient quality crystallization. For membrane proteins, however,

**Received:** September 16, 2011

**Revised:** October 31, 2011

**Published:** November 01, 2011

it is difficult to prepare (micro)crystalline samples. Aside from the preparation of microcrystalline samples, several techniques have been developed to prepare a membrane itself and a membrane protein with macroscopically homogeneous distribution in membranes. In mechanically glass-aligned samples of the membrane, samples are sandwiched between glass plates, and the glass plates are stacked. Then, NMR spectra were measured under static conditions.<sup>9–13</sup> Each resonance in the resulting NMR spectrum will be able to limit the line broadening, and furthermore, these chemical shift values reflect the orientation of the specific site of the molecules with respect to the membrane. In another approach, MAS is applied to oriented samples (i.e., magic angle-oriented sample spinning, MAOSS).<sup>14–16</sup> Membranes are sandwiched between small glass disks and stacked inside MAS rotors. The spectra obtained under MAS show impressive enhancement in line narrowing, as compared to the former approach, while still reserving orientation information with respect to the membrane. These methods have been established as essential for determining the molecular topology of membrane proteins and peptides.

In this study, we demonstrate the highly resolved <sup>13</sup>C CP MAS NMR spectrum of crystalline 1,2-dimyristoyl-*sn*-glycero-3-phosphocholine (DMPC). A high-field magnet (600 MHz) of NMR combined with improvement in the sample preparation method allowed us to obtain a highly resolved <sup>13</sup>C NMR spectrum. Crystalline DMPC samples with a defined hydration from DMPC multilamellar vesicle (MLV) dispersions were prepared using two novel approaches. One approach is preparation through drying under a nitrogen stream and thorough mixing with a spatula. The other is dehydrating on octadecyltriethoxysilane (OTS)-coated glass slides. We also examined the phase diagram of the low hydration level of DMPC ( $3 \leq n_w \leq 12$ ) through observation of the hydration level and temperature dependence of <sup>1</sup>H and <sup>13</sup>C NMR spectra of DMPC. We also achieved a complete <sup>1</sup>H/<sup>13</sup>C resonance assignment of the crystalline DMPC by combining MAS-J-Heteronuclear Multiple Quantum Coherence (MAS-J-HMQC) and frequency switched Lee–Goldburg heteronuclear shift correlation spectroscopy (FSLG-HETCOR) for unlabeled DMPC samples with two kinds of Dipolar Assisted Rotational Resonance (DARR) experiments for selectively <sup>13</sup>C1-labeled DMPC diluted with unlabeled DMPC. Finally, we calculated chemical shift values for the X-ray crystal DMPC structures and compared these to the assigned chemical shift values by solid-state NMR in this study. This study highlights the importance of adjusting the hydration level and temperature to obtain a crystalline phospholipid sample and provides us with chemical shift values and conformational information of two isomers in crystalline DMPC samples. The current method provides a possible application for highly resolved NMR spectra of membrane-associated proteins using microcrystalline samples.

## II. EXPERIMENTAL METHODS

**II.1. Materials.** DMPC (1,2-dimyristoyl-*sn*-glycero-3-phosphocholine) was purchased from Funakoshi (Tokyo, Japan) and used without further purification. Octadecyltriethoxysilane (OTS) was obtained from Shin-etsu Kagaku Co. (Japan). Dichloromethane and tetrahydrofuran (THF) were purchased from Nacalai Tesque (Kyoto, Japan). Hellmanex solution was purchased from Hellma (Mullheim, Germany).

**II.2. Preparation of Phospholipid Vesicles and Surface-Ordered Bilayers.** All samples except for those on OTS-coated

glass slides were prepared as follows. DMPC was directly mixed with H<sub>2</sub>O and extensively vortexed. The suspensions were freeze–thawed for 10 cycles and centrifuged. To create a low hydration state, the pellet was dried on a glass plate under a nitrogen stream and mixed thoroughly using a spatula until the bilayer became waxy. For FSLG-HETCOR and MAS-J-HMQC experiments, H<sub>2</sub>O was replaced with D<sub>2</sub>O. Buffers were not used in any of the samples.

Samples on OTS-coated glass slides were prepared as follows. DMPC was dissolved in chloroform/methanol (8:2 v/v); the solvent was evaporated; and then the film was further dried under a high vacuum overnight. After evaporation of the solvent, the lipid film was hydrated with deionized water and extensively vortexed. Then, 200  $\mu$ L of DMPC MLV dispersions were deposited on the surface of the glass slide. After equilibrating with the atmosphere overnight, the sample was placed in a sealed chamber containing silica gel for 5 days. The sample was then gradually dehydrated becoming first milky white and then waxy. When we preserved the samples, they were further equilibrated at room temperature in a sealed chamber containing a saturated solution of K<sub>2</sub>CO<sub>3</sub>, where a relative humidity (RH) of 44% was maintained.

The samples prepared by rapid mixing were transferred to an NMR rotor as they were, whereas samples on the OTS-coated glass slides were separated from the glass plate and diced to 1  $\times$  1 mm squares and then transferred to an NMR rotor. NMR rotors were capped with a drive tip having a sealing function (Phi Creative, Inc., Uji, Japan) to prevent dehydration.

**II.3. Preparation of OTS-Coated Glass Slides.** Glass slides were cleaned by sonicating in a 0.5% Hellmanex solution for 20 min and rinsing with deionized water. They were further treated in a cleaning solution of 0.05:1:5 NH<sub>4</sub>OH (28%)/H<sub>2</sub>O<sub>2</sub> (30%)/H<sub>2</sub>O for 10 min at 65  $^{\circ}$ C and rinsed again extensively with deionized water. They were subsequently dried in a vacuum oven for 30 min at 80  $^{\circ}$ C. OTS solution was prepared by mixing 0.2 mL of 1 M HCl solution, 25 mL of tetrahydrofuran (THF), and 0.2 mL of OTS and stirred for a few days (>48 h) to hydrolyze the OTS. After membrane filtering, the solution was mixed with 80 mL of cyclohexane. Next, clean glass slides were immersed into the OTS solution for 20 min. The self-assembled monolayers of OTS (OTS-SAM) were then rinsed twice with a mixture of dichloromethane and acetone (1:1) to remove unreacted silane and twice with deionized water. The OTS-SAM was cross-linked in a vacuum oven at 110  $^{\circ}$ C for 1 h. After cooling at room temperature, OTS-coated glass slides were sonicated twice in cyclohexane for 5 min to remove remaining physisorbed OTS clusters. They were finally dried in a vacuum oven at 90  $^{\circ}$ C for 30 min and cooled at room temperature.

**II.4. Solid-State NMR Spectroscopy.** All solid-state NMR spectra were acquired on a Bruker Avance 600 spectrometer (Bruker Biospin, Billerica, MA) equipped with a narrow-bore magnet operating at a resonance frequency of 150.13 MHz for <sup>13</sup>C and 600.13 MHz for <sup>1</sup>H. All experiments were recorded with an E-free 4 mm triple-resonance MAS probe, at spinning speeds of 10 kHz. The 1D <sup>1</sup>H spectra were collected with 4  $\mu$ s excitation pulses and a 1 s recycle delay. The 1D <sup>13</sup>C cross-polarization (CP) MAS spectra were acquired using a proton excitation pulse length of 4  $\mu$ s and a 2 ms contact time with 66 kHz SPINAL-64 <sup>1</sup>H decoupling<sup>17</sup> during acquisition. For CP, a ramped (from 50 to 100%) spin-lock pulse on the proton channel and square contact pulse on the <sup>13</sup>C channel were used. Recycle delay was set to 5 s. The 2D MAS-J-HMQC experiment<sup>18,19</sup> was obtained by recording 70  $t_1$  increments with 2048 scans each. The evolution

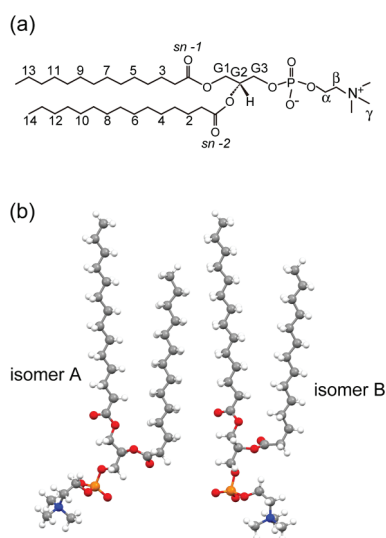


**Figure 1.** (a) Chemical structure of DMPC with nomenclature. (b) Optimized structure of the two isomers, A and B, in a unit cell of the DMPC crystal with proton coordinates and further amine moieties using Gaussian 98 (B3LYP functional, 6-31G(d,p) basis). The molecular structure is first built up by the MM method referring to dihedral angles reported by a crystal structure study determined by X-ray scattering.<sup>27</sup> Carbon atoms are gray, oxygen atoms are red, phosphorus atoms are orange, nitrogen atoms are blue, and hydrogen atoms are white.

period was 2.3 ms, and it was synchronized to be an integral number of rotor periods. The proton RF field strength was set to 66 kHz during both the  $t_1$  revolution period (FSLG decoupling)<sup>20</sup> and acquisition (SPINAL-64 decoupling). The repetition delay was 3 s. The 2D FSLG-HETCOR experiment<sup>21</sup> was obtained by recording 80  $t_1$  increments with 1024 scans each. The proton RF field strength was set to 66 kHz during both the  $t_1$  revolution period (FSL decoupling) and acquisition (TPPM decoupling with a 15° phase increment). The recycle delay was set to 3.7 s. 2D dipolar-assisted rotational resonance (DARR) NMR spectra<sup>22–24</sup> for selectively  $^{13}\text{C}1$ -labeled DMPC/unlabeled DMPC (1/10) (Figure 5) were recorded with 800 hypercomplex points in the indirect dimension with a mixing time of 0, 50, and 100 ms during which the proton field was adjusted to the spinning frequency of 10 kHz and 32 scans each. The recycle delay was set to 5 s. For selectively  $^{13}\text{C}1$  labeled DMPC/unlabeled DMPC (1/5) (Figure 6), 600 hypercomplex points were acquired in the indirect dimension with a mixing time of 100 ms and 512 scans each. The recycle delay was set to 3.5 s. For all 2D experiments, ramped CP was used with the same conditions we used in 1D  $^{13}\text{C}$  CP-MAS experiments. All  $^{13}\text{C}$  spectra were processed using 0.3 Hz line broadening. The actual temperature in the sample under 10 kHz MAS was calibrated using chemical shift differences between the water and methyl peaks in the low hydrated DMPC sample.<sup>25</sup> All temperatures quoted are the calibrated temperatures. The  $^1\text{H}$  and  $^{13}\text{C}$  chemical shifts were externally referenced to the methine carbon of adamantane (29.5 ppm).<sup>26</sup>

**II.5. Quantum Chemical Calculations.** Calculations of the chemical shift for the crystal DMPC structures reported by Pearson and Pascher were performed using GIAO at the hybrid density function theory (DFT) level. First, we built two models (isomers A and B) referring to dihedral angles reported by a crystal structure study.<sup>27</sup> Three-dimensional structures were optimized at the MM level. The geometries of hydrogens and

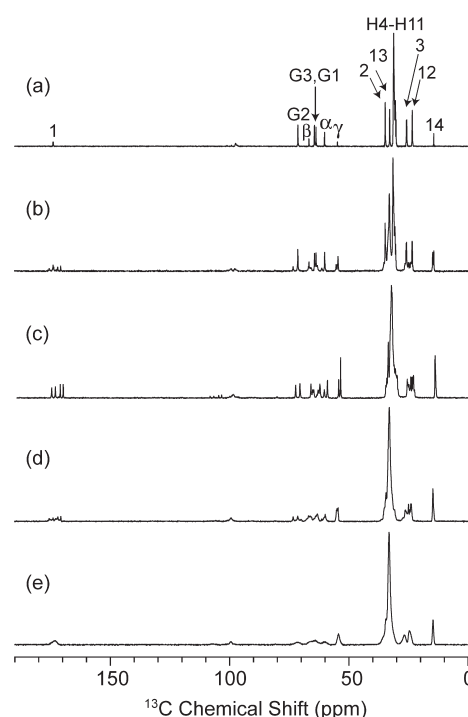


**Figure 2.**  $^{13}\text{C}$  CP-MAS NMR spectra of DMPC at 307 K with varying water/lipid ratios,  $n_W = 11$  (a), 6 (b), 4 (c), and 3 (d) and in a lyophilized state (e). The DMPC  $^{13}\text{C}$  assignment is indicated in (a). 512 FIDs were accumulated for each experiment. Spectra were processed using a 0.3 Hz line broadening.

the amine moiety were optimized using a B3LYP exchange correlation function with 6-31G(d,p). NMR chemical shifts relative to the TMS for those optimized models were calculated at the GIAO-B3LYP/6-311++G(d,p). To clarify the effect of two bound water molecules for the NMR chemical shift, we optimized each complex consisting of two water molecules and either isomers A or B at B3LYP/6-31G(d,p) and calculated the chemical shifts at the GIAO/B3LYP/6-311++G(d,p). The resulting chemical shift values were almost identical to those without the water molecules. Therefore, we chose the isomer A and B unbinding waters as the models for the calculation of the chemical shifts that allowed us to optimize the bond angles and distances of those two models at the B3LYP/6-31H(d,p) level. Molecular structures under such optimization are shown in Figure 1b. Nuclear shieldings relative to the TMS were also computed at the B3LYP/6-311++G(d,p). All DFT calculations were performed with the Gaussian 03 program suite.<sup>28</sup>

### III. RESULTS

#### III.1. Phase Diagram of the Low Hydration Level of DMPC.

We first demonstrated the results of the samples that were prepared by drying DMPC MLV dispersions on the glass plate under a nitrogen gas stream and mixing thoroughly with a spatula. Figure 2 shows the  $^{13}\text{C}$  NMR spectra of DMPC at 307 K with varying water/lipid ratios,  $n_W = 11$  (a), 6 (b), 4 (c), and 3 (d) and in the lyophilized state (e). Spectral patterns changed drastically depending on the hydration level. At  $n_W = 11$  (Figure 2a), the spectrum showed a typical spectral pattern of the lamellar phase ( $L_\alpha$ ) of DMPC.<sup>29,30</sup> At  $n_W = 4$  (Figure 2c), all resonances were as sharp as those shown in Figure 2a in spite of the low hydration level. Interestingly, the number of signals



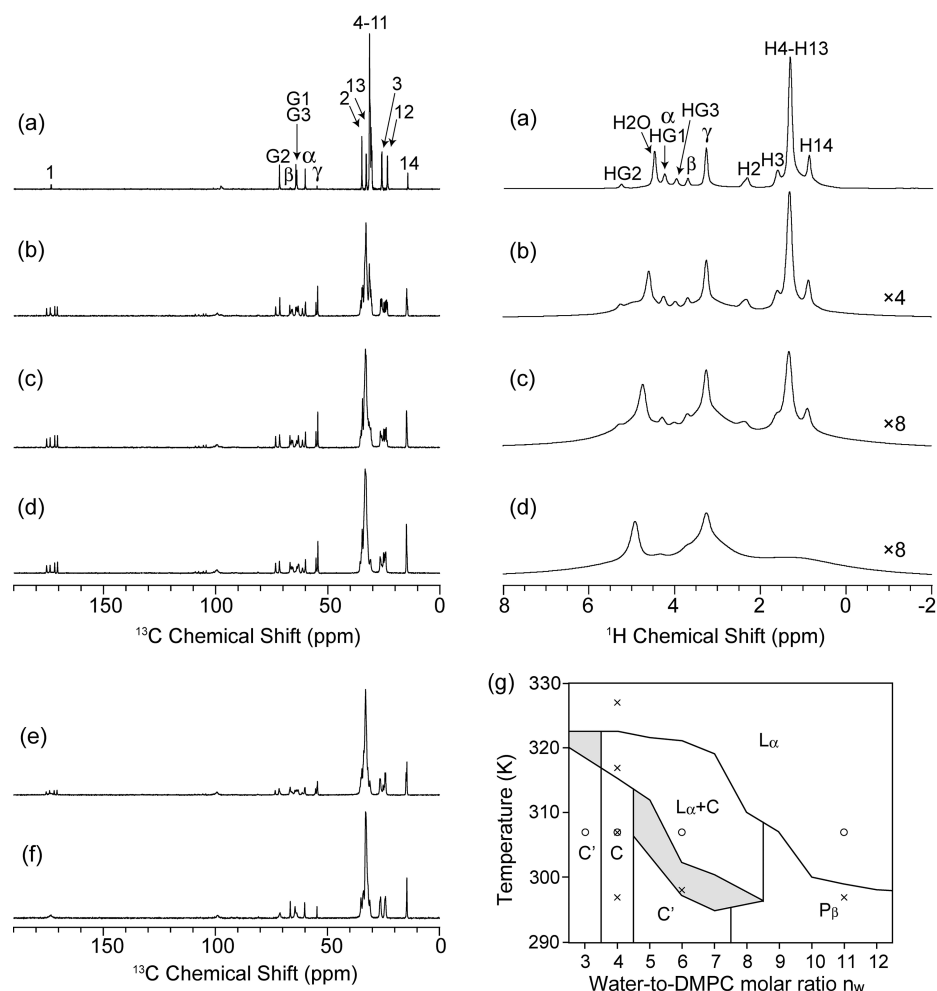


**Figure 3.** (a–d)  $^{13}\text{C}$  CP-MAS (left column) and  $^1\text{H}$  MAS (right column) NMR spectra of DMPC at  $n_W = 4$  at various temperatures (a) 327, (b) 317, (c) 307, and (d) 297 K. The DMPC  $^{13}\text{C}$  and  $^1\text{H}$  assignments are indicated in (a). (e, f) The  $^{13}\text{C}$  CP-MAS NMR spectra of DMPC at  $n_W = 6$  and 299 K (e) and at  $n_W = 11$  and 297 K (f). (g) Temperature–water/lipid ratio  $n_W$  phase diagram of hydrated DMPC for  $n_W$  between 3 and 12. Gray regions show the conformational distributed mixed phase,  $(L_\alpha + C)'$ . ○ and × indicate the condition of temperature and  $n_W$  at which we observe the spectra shown in Figures 2 and 3, respectively. All  $^{13}\text{C}$  spectra were obtained and processed as described in Figure 2.

shown in Figure 2c was almost twice that shown in Figure 2a. These results indicate that DMPC takes a crystalline state (C), having two distinct forms of conformations in one unit cell at  $n_W = 4$ . At  $n_W = 6$  (Figure 2b), a mixture of the lamellar phase (Figure 2a) and crystalline phase (Figure 2c) spectrum pattern components was observed, indicating the coexistence of these two phases ( $L_\alpha + C$ ). At  $n_W = 3$  (Figure 2d), spectra showed line broadening of the spectral pattern in Figure 2c ( $C'$ ). This appears to result from a mosaic spread of the orientation of DMPC molecules from a crystalline state at  $n_W = 4$ . In the lyophilized state (Figure 2e), each peak became further broadened compared to those in Figure 2d.

Figures 3a–d show the  $^{13}\text{C}$  CP (left column) and  $^1\text{H}$  (right column) MAS NMR spectra of DMPC at  $n_W = 4$  and at various temperatures. At 327 K (Figure 3a), the  $^{13}\text{C}$  spectrum indicates that DMPC takes the lamellar state ( $L_\alpha$ ) at higher temperatures even at  $n_W = 4$ . At 317 K (Figure 3b), the  $^{13}\text{C}$  spectrum showed an almost crystalline phase spectral pattern, but lamellar phase components were mingled in a little ( $L_\alpha + C$ ). At 307 K (Figure 3c) and 297 K (Figure 3d), the  $^{13}\text{C}$  NMR spectra showed the spectrum pattern of the crystalline phase (C).

Generally, the gel to liquid crystalline transition temperature of phospholipids has been known to be extremely sensitive to the hydration level; from a  $n_W$  of ten to one,  $T_m$  is gradually elevated as has been reported for a variety of lipids.<sup>31–34</sup> The change of the  $^{13}\text{C}$  CP-MAS NMR spectral pattern suggests that the  $T_m$  of the DMPC at  $n_W = 4$  resulted from the low hydrated condition. By closely examining the change of the  $^{13}\text{C}$  CP-MAS NMR spectral pattern, the transition temperature from the mixed phase ( $L_\alpha + C$ ) to the lamellar phase ( $L_\alpha$ ),  $T_{mv}$  of DMPC at  $n_W = 4$  was found to be 323 K. (Hereafter, chain melting transition temperatures to the lamellar phase are expressed as  $T_m$ .) The chemical shift values were also drastically changed in fatty acid chains between crystalline and lamellar phases. This results from fatty acid chains being all-trans in the crystalline phase and also being trans–gauche in the lamellar phase. On the other hand, even though the line width of the  $^1\text{H}$  MAS NMR spectrum (Figure 3a, right column) drastically changed as temperature decreased, the chemical shift values barely changed except for the  $\text{H}_2\text{O}$  peak. Above  $T_m$ , the  $^1\text{H}$  NMR spectral pattern also showed the spectral pattern of DMPC in the lamellar phase, which was previously assigned by Mei et al.<sup>29</sup> By fitting the  $^1\text{H}$  MAS NMR spectrum

line above  $T_m$  using gNMR (version 5.0)<sup>35</sup> and ratioing the peak areas of H<sub>2</sub>O and other lipid peaks, we can see that the water/lipid ratio  $n_W$  is 4. In this study, all water/lipid ratios,  $n_W$ , were determined in such a manner.

To examine the phase diagram of the low hydration level of DMPC, we measured the <sup>13</sup>C CP-MAS and <sup>1</sup>H MAS NMR spectra at various temperatures (290 K <  $T$  < 330 K) and  $n_W$  ( $3 \leq n_W \leq 12$ ). We were able to see the conformational distributed mixed phase ( $(L_\alpha + C)'$ ) (Figure 3e, at  $n_W = 6$  and 299 K) and ripple phase ( $P_\beta$ ) (Figure 3f, at  $n_W = 11$  and 297 K) in this range, except for  $L_\alpha$ ,  $C$ ,  $L_\alpha + C$ , and  $C'$  phases. In Figure 3f, glycerol and acyl chain carbon signals broadened compared to those in the lamellar phase ( $L_\alpha$ ) (Figures 2a and 3a), suggesting that the motion of these carbons became slower than in the  $L_\alpha$  phase. Although we were unable to distinguish the <sup>13</sup>C CP-MAS NMR spectra of the ripple phase ( $P_\beta$ ) and the gel phase ( $L_\beta$ ) due to their similarity, we tentatively regarded the spectrum in Figure 3f as that of the  $P_\beta$  phase based on the fact that the hydrated DMPC bilayers changed their phase from the  $L_\alpha$  to the  $P_\beta$  phase and then to the  $L_\beta$  phase. We summarized these results in a tentative phase diagram (Figure 3g). At  $n_W < 3$ , the sample changed to a powder-like state, and it was difficult to remove two waters per one DMPC molecule by drying under a nitrogen gas stream. Therefore, we made this phase diagram in the range of  $3 \leq n_W \leq 12$ . It clearly shows that DMPC took the crystalline state at the narrowly restricted condition,<sup>36</sup> around  $n_W = 4$  and  $T < 313$  K (within our measured range). The crystalline phase was too stable, and orientation did not distribute easily even at low temperature. At  $n_W = 3$ , DMPC took a similar phase state at  $n_W = 4$ , whereas the orientation was a little distributed. Above  $n_W = 9$ , DMPC was in the  $L_\alpha$  phase above  $T_m$  (Figure 3a) and in the ripple phase below  $T_m$  (Figure 3f). At  $n_W = 5-8$ , DMPC took a mixed phase ( $L_\alpha + C$ ) below  $T_m$ . The orientation became distributed ( $(L_\alpha + C)'$ ) as the temperature decreased, ending in a phase shift to the conformational distributed crystalline phase  $C'$ . The phase diagram in Figure 3g was based on <sup>13</sup>C CP-MAS NMR spectra at various temperatures and hydration levels. However, since these samples were rather rapidly prepared by dehydration under a nitrogen stream, it is possible that some samples remained in their metastable state. Although this phase diagram generally agrees with those reported previously, it might differ slightly from a truly equilibrated diagram.

**III.2. Assignment of the <sup>13</sup>C and <sup>1</sup>H NMR Spectra.** To perform comprehensive <sup>1</sup>H/<sup>13</sup>C NMR assignment of the crystalline DMPC spectra at  $n_W = 4$ , we have obtained some correlation spectra as follows. Figure 4a shows the one-bond MAS-J-HMQC spectrum of the DMPC measured at 307 K. The expanded region of the head group and glycerol signal (from 53 to 75 ppm) in Figure 4a is also shown in red in Figure 4c. Referring to the <sup>1</sup>H chemical shift values in Figure 3d (right column), the carbon chemical shift directly bonded to the protons ( $\omega_{13C}$ ,  $\omega_{1H}$ ) could be easily identified from the one-bond MAS-J-HMQC spectrum, such as  $\alpha$  or G1 [(59.9 ppm, 4.36 ppm) and (61.3 ppm, 4.31 ppm)],  $\beta$  [(65.7 ppm, 3.61 ppm) and (66.9 ppm, 3.61 ppm)],  $\gamma$  [(54.5 ppm, 3.16 ppm) and (55.2 ppm, 3.24 ppm)], G2 (71.4 ppm, 5.12 ppm), and G3 (63.9 ppm, 3.84 ppm). Although the <sup>1</sup>H chemical shift value of the correlation peak that appeared at ( $\omega_{13C}$ ,  $\omega_{1H}$ ) = (73.3 ppm, 5.70 ppm) is not shown in Figure 3d (right column), we tentatively assigned it as another G2 cross peak estimated from typical chemical shift values. The cross peaks for acyl chains were also roughly assigned. Assignments are shown in Figure 4a and 4c. It is important to note that at this stage we were

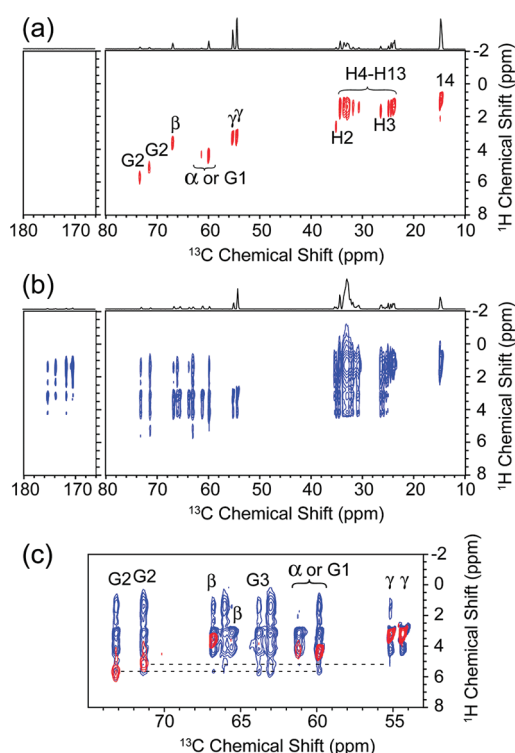


**Figure 4.** (a) 2D <sup>1</sup>H/<sup>13</sup>C MAS-J-HMQC and (b) dipolar HETCOR NMR spectra of DMPC at 307 K, respectively. For (b), 2 ms contact times were used. (c) The superimposition of expanded regions of the head group and glycerol signals (from 53 to 75 ppm) in (a) and (b). The threshold level of both spectra in (c) is set lower than in (a) and (b). The assignments from 2D <sup>1</sup>H/<sup>13</sup>C MAS-J-HMQC are indicated in (a) and (c).

not able to identify which isomers these peaks were derived from. Due to the lack of directly bonded protons to the carbonyl carbon, a cross peak is not observed for the C1 carbons.

To assign which carbonyl peaks are from each isomer, we measured a series of 2D <sup>13</sup>C–<sup>13</sup>C NMR correlation spectra collected at 315 K with increasing DARR mixing times with selectively <sup>13</sup>C1-labeled DMPC/unlabeled DMPC (1/10) (Figure 5). At a mixing period of 50 ms (Figure 5b), cross peaks due to magnetization transfer between <sup>13</sup>C spins during the mixing period were observed between 175.4 and 171.8 ppm. At a mixing period of 100 ms (Figure 5c), these cross peaks became bigger, and additional smaller cross peaks were observed between 173.8 and 170.6 ppm. These peaks must be cross peaks originating from intramolecular dipolar interaction between *sn*-1 and *sn*-2 C1 carbons because <sup>13</sup>C1-labeled DMPC was diluted by unlabeled DMPC in this sample. Here, we denote individual DMPC conformations in the crystalline state by the letters I and II and assume that strong correlation peaks ( $\omega_{13C}$ ,  $\omega_{13C}$ ) = (175.4 ppm, 171.8 ppm) arose from intramolecular dipolar interactions between *sn*-1 and *sn*-2 C1 carbons in isomer I, and weak correlation peaks ( $\omega_{13C}$ ,  $\omega_{13C}$ ) = (173.8 ppm, 170.6 ppm) were from these in isomer II.

Figure 6 shows the cross-sectional slices extracted at each position of the C1 carbon resonance of 2D <sup>13</sup>C–<sup>13</sup>C NMR correlation spectra collected at 315 K with 100 ms DARR mixing times with selectively <sup>13</sup>C1-labeled DMPC/unlabeled DMPC (1/5). Since this experiment aimed to identify close carbons from each C1, large cross peaks are predictable for *sn*-1 C1 with CG1

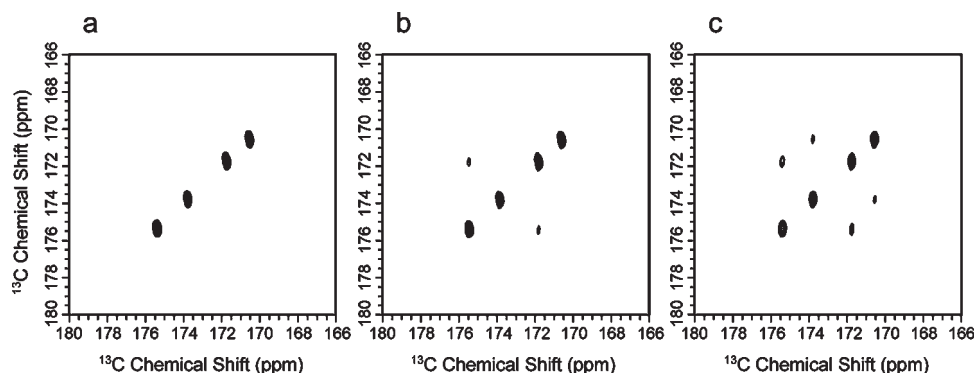


**Figure 5.** Expanded region of the C1 group signals (from 166 to 180 ppm) of 2D  $^{13}\text{C}/^{13}\text{C}$  correlation spectra of selectively  $^{13}\text{C}_1$ -labeled DMPC/unlabeled DMPC (1/10) collected with different DARR mixing periods: (a) 0, (b) 50, and (c) 100 ms. Spectra were obtained with 10 kHz MAS and DARR conditions of  $n = 1$  ( $\omega_1 = \omega_R$ ).

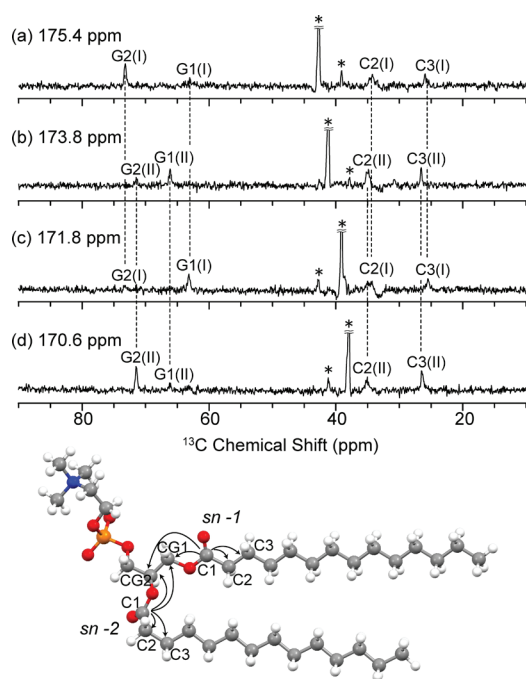


**Figure 6.** C1 slices extracted from the F1 dimension of the  $^{13}\text{C}-^{13}\text{C}$  2D DARR spectrum with a 100 ms DARR mixing period. Slices were obtained at four different C1 resonances: (a) 175.6, (b) 173.8, (c) 171.8, and (d) 170.6 ppm. Spinning side bands of C1 resonances are denoted with asterisks. The assignments clarified from these spectrum slices are indicated. Correlations in the above spectra are given by arrows in the bottom DMPC molecule.

and *sn*-2 C1 with CG2 and for all C1 with C<sub>2</sub>. We observed the two large cross peaks between C1 and CG2 at ( $\omega_{^{13}\text{C}}$ ,  $\omega_{^{13}\text{C}}$ ) = (175.4 ppm, 73.3 ppm) and (170.6 ppm, 71.4 ppm). The remaining two large cross peaks at (173.8 ppm, 66.2 ppm) and (171.8 ppm, 63.2 ppm) were thus identified as the cross peaks between C1 and CG1. Therefore, 175.4 and 171.8 ppm peaks were assigned to *sn*-2 and *sn*-1 C1 carbons in conformation I, respectively. As well, 173.8 and 170.6 ppm peaks were assigned to *sn*-1 and *sn*-2 C1 carbons in conformation II, respectively. Furthermore, we easily assigned cross peaks between each C1 peak and CG1, CG2, C<sub>2</sub> (one bond apart), and C<sub>3</sub> (two bonds apart) carbons (see Figure 6, Tables 1 and 2).

**Table 1.**  $^{13}\text{C}$  Chemical Shifts in Parts per Million of Crystalline DMPC at  $n_W = 4$  Assigned by NMR

assignment	isomer I	isomer II	X-ray study <sup>a</sup>
C1	171.8 ( <i>sn</i> -1), 175.4 ( <i>sn</i> -2)	173.8 ( <i>sn</i> -1), 170.6 ( <i>sn</i> -2)	175.0, 173.9, 173.2, 171.4
C2	34.4	35.1	na
C3	25.45 ( <i>sn</i> -1), 25.9 ( <i>sn</i> -2)	26.4	na
C4–12	33.0 (t), 30.7 (g) <sup>b</sup>	33.0 (t), 31.9 (g) <sup>b</sup>	na
C13	24.9 (t), 24.4 (g) <sup>b</sup>	24.0 (t), 23.8 (g) <sup>b</sup>	na
C14	14.7	14.7	na
G1	63.2	66.2	na
G2	73.3	71.4	74.2, 69.7
G3	63.9	63.2	62.8, 61.45
$\alpha$	59.9	61.3	61.0, 60.1
$\beta$	66.9	65.7	na
$\gamma$	54.4	55.2	na

<sup>a</sup>  $^{13}\text{C}$  chemical shift values for type I samples are referred from Bruzik and Harwood. <sup>b</sup> t and g show trans and gauche conformations in acyl chains.

**Table 2.**  $^1\text{H}$  Chemical Shifts in Parts per Million of DMPC at  $n_W = 4$  Assigned by NMR<sup>a</sup>

assignment	isomer I	isomer II
H2	2.76	2.59
H3	1.57	1.64
H4–13	1.38	1.38
H14	0.95	0.95
HG1	4.46	4.35
HG2	5.70	5.12
HG3	3.84	3.67
H $\alpha$	4.36	4.31
H $\beta$	3.61	3.61
H $\gamma$	3.16	3.24

<sup>a</sup> The center position of the signal is reported here.

The 2D  $^{13}\text{C}-^1\text{H}$  FSLG-HETCOR spectrum of the unlabeled DMPC measured at 315 K is shown in Figure 4b. We were able to observe many additional peaks present due to long-range transfer

compared to Figure 4a. The expanded region of the head group and glycerol signal (from 53 to 75 ppm) shown in Figure 4b is also shown in blue in Figure 4c. This was superimposed on the expanded region of Figure 4a. The cross peaks appearing on the broken line in Figure 4c allowed us to identify  $C\alpha$  (59.9 ppm),  $C\beta$  (66.9 ppm), and  $C\gamma$  (54.4 ppm) peaks as peaks of conformation I and  $C\alpha$  (61.3 ppm),  $C\beta$  (65.7 ppm), and  $C\gamma$  (55.2 ppm) peaks as peaks of conformation II. For G3, we found only one cross peak in the expanded MAS-J-HMQC spectrum (Figure 4c) at  $(\omega_{13C}, \omega_{1H}) = (63.9 \text{ ppm}, 3.84 \text{ ppm})$ . In the expanded region of the  $^{13}\text{C}$ – $^1\text{H}$  FSLG-HETCOR spectrum (Figure 4c), the correlation peak was also observed between the CG3 carbon (63.9 ppm) and the HG2(I) proton (5.70 ppm), suggesting that the CG3 carbon (63.9 ppm) is most likely from conformation I. On the other hand, two peaks overlapped at 63.2 ppm in the  $^{13}\text{C}$  CP-MAS spectrum (Figure 2c). One was already assigned as CG1(I), and the other was able to be assigned as CG3 of isomer II. In Figure 4c, there is a cross peak at  $(\omega_{13C}, \omega_{1H}) = (63.2 \text{ ppm}, 5.70 \text{ ppm})$  and also at  $(\omega_{13C}, \omega_{1H}) = (63.2 \text{ ppm}, 5.12 \text{ ppm})$ . These cross peaks allow us to confirm that the former one was between CG1(I) and HG2(I) as mentioned above and

**Table 3. Calculated  $^{13}\text{C}$  Chemical Shifts in Parts per Million of DMPC for the X-ray Crystal DMPC Structure Reported by Pearson and Pascher**

assignment	isomer A	isomer B
C1 <i>sn</i> -1	183.43	181.91
C1 <i>sn</i> -2	182.27	179.81
C2	39.20 ( <i>sn</i> -1), 39.64 ( <i>sn</i> -2)	40.89 ( <i>sn</i> -1), 39.54 ( <i>sn</i> -2)
C3	31.15 ( <i>sn</i> -1), 35.16 ( <i>sn</i> -2)	32.88 ( <i>sn</i> -1), 33.79 ( <i>sn</i> -2)
C4–12 <sup>a</sup>	36.76–40.14 ( <i>sn</i> -1), 35.34–39.86 ( <i>sn</i> -2)	37.74–39.46 ( <i>sn</i> -1), 34.15–39.98 ( <i>sn</i> -2)
C13	30.21 ( <i>sn</i> -1), 29.43 ( <i>sn</i> -2)	29.79 ( <i>sn</i> -1), 30.18 ( <i>sn</i> -2)
C14	17.66 ( <i>sn</i> -1), 17.84 ( <i>sn</i> -2)	17.42 ( <i>sn</i> -1), 17.49 ( <i>sn</i> -2)
G1	72.38	66.54
G2	77.33	78.85
G3	66.28	68.71
$\alpha$	62.43	60.41
$\beta$	75.45	77.55
$\gamma$	58.98	58.61

<sup>a</sup> For C4–12, we only describe the range of chemical shift values.

the latter one was between CG3 (II) and HG2(II). The cross peaks for acyl chains were assigned from 2D  $^{13}\text{C}$ – $^1\text{H}$  one-bond MAS-J-HMQC and FSLG-HETCOR spectra. All assignments are shown in Tables 1 and 2.

**III.3. Comparison between Assigned and Calculated Chemical Shift Values.** We calculated the chemical shifts from ab initio theory to compare the assigned chemical shift values from solid-state NMR (Table 1) and calculated values for the X-ray crystal structures of DMPC (isomers A and B) (Figure 1b). The calculated  $^{13}\text{C}$  chemical shift values for isomers A and B are listed in Table 3. Figure 7a shows a comparison between the glycerol and head group regions of the putative spectra created using the calculated and experimental  $^{13}\text{C}$  NMR chemical shift values, respectively. All calculated values were deshielded. In particular,  $C\beta$  in both isomers showed large downfield shifts in calculated values. However, the relative relationships of chemical shift values between specific carbons in each conformation were almost reproduced with the same relative relationship. This result convinced us that conformations I and II of crystalline DMPC correspond to conformations B and A in X-ray crystalized DMPC, respectively. Figure 7b shows the correlation plots between the calculated and experimental chemical shift. The correlation plots showed a smaller root-mean-square deviation (rmsd) in isomer A and II (2.71) than in isomer A and I (3.05), and the same was seen in isomer B and I (3.42) when compared with isomer B and II (4.25). From these results, we assessed that conformations I and II of crystalline DMPC in our study

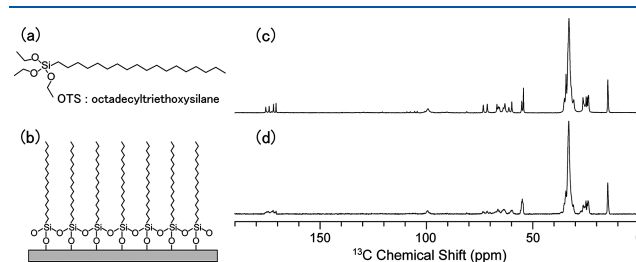


**Figure 8.** (a) Chemical structure of octadecyltriethoxysilane (OTS). (b) Schematic representation of the OTS-coated glass slide. (c, d) The  $^{13}\text{C}$  CP-MAS NMR spectra of DMPC bilayers obtained after sample dehydration on (c) an OTS-coated glass slide and (d) a non-OTS-coated glass slide. Spectra were processed using a 0.3 Hz line broadening.

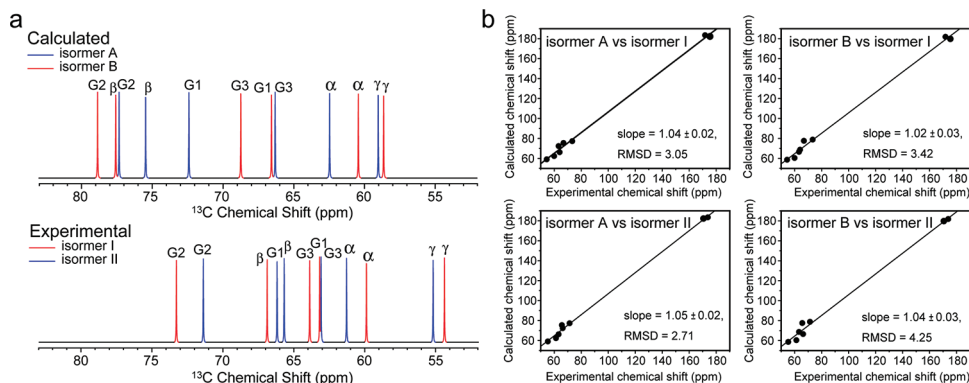


**Figure 7.** (a) Glycerol and head group region of the putative spectra created using the calculated  $^{13}\text{C}$  NMR chemical shift values and the experimentally assigned chemical shift values in this study. (b) Calculated (isomers A and B) and experimental (isomers I and II) chemical shift correlation plot with linear fitting. Values of the slope of linear fitting and root-mean-square deviation (rmsd) are described in the graph. The C2–12 moiety in the acyl chain was not plotted.



correspond to conformations B and A, respectively, in the X-ray structure of DMPC.

**III.4. OTS-Coated Glass Aligned DMPC.** Coating with a self-assembled monolayer (SAM) of octadecyltriethoxysilane (OTS, Figure 8a) is a useful technique for modifying glass or silicone surfaces and has utility in a large number of applications.<sup>37,38</sup> Since an OTS-coated substrate has a layer of long alkane chains on the surface, phospholipid monolayers can be aligned on it, facing the hydrophobic chains to the substrate.<sup>39</sup> To make crystalline DMPC by drying the sample from DMPC MLV dispersions (without mixing), we prepared crystalline DMPC on an OTS-coated glass slide. The  $^{13}\text{C}$  NMR spectrum of DMPC bilayers obtained after sample dehydration on the OTS-coated glass slide (Figure 8b) at 307 K is shown in Figure 8c. We were able to obtain the same spectral pattern of the crystalline state of DMPC as shown in Figure 2c. The value of  $n_W$  for the OTS-coated glass aligned DMPC sample was found to be 3 from the  $^1\text{H}$  MAS NMR spectrum. When preparing the DMPC sample at  $n_W = 3$  by sample preparation by rapid mixing, we found conformational distribution from the crystalline state on the basis of the  $^{13}\text{C}$  NMR spectral pattern. This result thus indicates that if we prepare samples to be in their equilibrium state, like an OTS-coated glass aligned DMPC sample, DMPC would take the crystalline state, even except for at  $n_W = 4$ . For comparison, the  $^{13}\text{C}$  NMR spectrum of DMPC bilayers, obtained after sample dehydration on a non-OTS-coated glass slide at 307 K, is presented in Figure 8d. The resonance pattern was similar to that seen in Figure 8c; however, the resonance line width was broader for almost all resonances. This line broadening most likely originated from the mosaic spread of the orientation of the DMPC molecules. Thus, these results clearly indicate that OTS coating (Figure 8b) has a strong effect on molecular ordering on the glass slide.

## IV. DISCUSSION

Conformational heterogeneity in the low hydration level brings about inhomogeneous line broadenings in solid-state NMR spectra. The aim of our study was to acquire highly resolved solid-state  $^{13}\text{C}$  NMR spectra of phospholipid membranes by eliminating the conformational distribution of phospholipid molecules.

The  $^{13}\text{C}$  NMR spectra of DMPC with varying water ratios (Figure 2) indicated that DMPC molecules form a highly ordered, crystalline state at  $n_W = 4$ . The current observation that the number of signals was almost doubled compared with the spectrum at a higher hydration led us to suggest that this sample took two distinct conformations. The X-ray crystal structure of DMPC has shown two inequivalent molecular conformations (isomers A and B) in a unit cell.<sup>27</sup> Bruzik and Harwood demonstrated a  $^{13}\text{C}$  NMR spectrum of the DMPC crystal that closely resembled this crystal.<sup>40</sup> The  $^{13}\text{C}$  NMR spectral pattern of the DMPC crystal obtained at  $n_W = 2$  was similar to that of the present study at  $n_W = 4$  (Figure 2c). This suggests that the crystalline DMPC at  $n_W = 4$  takes two kinds of conformations similar to the crystal structure reported in the X-ray study. There were some differences observed in both  $^{13}\text{C}$  NMR spectra that we will discuss later.

The  $^{13}\text{C}$  CP-MAS and  $^1\text{H}$  MAS NMR spectra of DMPC at  $n_W = 4$  and at various temperatures (Figure 3a–d) indicated phase changes from the crystalline phase (C) to a mixed phase ( $L_\alpha + \text{C}$ ) and further to a lamellar phase ( $L_\alpha$ ), as the temperature rises.

The phase diagram of DMPC at  $3 \leq n_W \leq 12$  and at  $290 \text{ K} < T < 330 \text{ K}$  (Figure 3g) showed that DMPC takes a crystalline state only at  $n_W = 4$  and  $T < 313 \text{ K}$ . DMPC also took a crystalline state at  $n_W = 3$  when we prepared the DMPC sample by simply dehydrating it on an OTS-coated glass slide. In the X-ray crystal study of DMPC, single crystals were obtained at  $n_W = 2$  by recrystallization from an ether/ethanol/water solution.<sup>27</sup> Therefore, the conditions for  $n_W$  to form a crystalline state should be broader than that shown in the phase diagram in Figure 3g, depending on the sample preparation methods.

$^2\text{H}$  solid-state NMR spectra of some kinds of phosphatidylcholine (PC) MLVs recorded at different levels of hydration have demonstrated that  $^2\text{H}$  quadrupole splittings for the  $\alpha$ ,  $\beta$ , or  $\gamma$  segment of the choline head group of PC change drastically from  $n_W = 4$  to 10.<sup>31,33,34</sup> By analyzing quadrupole splittings vs  $n_W$  curve, it has been found that water molecules are tightly bound to the phospholipid until  $n_W = 4$  and can stay moderately bound up to  $n_W = 10$ . This tendency correlates well with the phase diagram proposed in this study. Tightly bound water molecules probably allowed DMPC to form a crystalline state at  $n_W = 4$ . In addition, at  $10 < n_W$ , since water molecules can not be bound to DMPC any further, the phase diagram would not change in this region.

Janiak et al. investigated the phase behavior of hydrated DMPC utilizing differential scanning calorimetry and X-ray diffraction methods. They reported the existence of a crystalline phase of DMPC at  $n_W = 4$ –6 and  $T = 300$ –308 K and two phase regions between the lamellar phase and crystalline phase.<sup>36</sup> Our results generally agree with these results in spite of using different methods to determine the phase behaviors. At a higher temperature, DMPC takes the lamellar phase ( $L_\alpha$ ) at all hydration levels. The phase transition temperature  $T_m$  to the lamellar phase ( $L_\alpha$ ) from one of the lower-temperature phases, i.e., ( $L_\alpha + \text{C}$ )' at  $n_W = 3$ ,  $L_\alpha + \text{C}$  at  $4 \leq n_W \leq 8$ , and  $\text{P}_\beta$  at  $9 \leq n_W$ , decreased as the water/lipid ratio  $n_W$  increased. This tendency was also reported by Janiak et al. Faure et al. have also investigated the  $T_m$  of DMPC using  $^2\text{H}$  solid-state NMR and showed that  $T_m$  decreases as the water/lipid ratio increases. However, in their report, they expressed  $T_m$  as a transition temperature from the gel to  $L_\alpha$  at  $n_W < 10$  and from  $\text{P}_\beta$  to  $L_\alpha$  at  $10 \leq n_W$ . Compared to their results, our results showed a higher  $T_m$  for each  $n_W$ . Such a difference appears to result from the difficulties of distinguishing the mixed phase state and gel state by  $^2\text{H}$  solid-state NMR. On the other hand, we were able to distinguish different phase states and quantify their ratio from the pattern of  $^{13}\text{C}$  NMR spectra. This is an advantage of analyzing the phase behaviors by the  $^{13}\text{C}$  NMR spectra.

At 307 K, there were four kinds of carbonyl carbon peaks for the crystalline DMPC at  $n_W = 4$  (Figure 2c), while it became only one peak above  $n_W \geq 9$  (Figure 2a). At the fully hydrated state, DMPC takes one conformation, and the  $^{13}\text{C}$  NMR spectrum should have two C1 peaks if the two C1 groups are fully rigid. Having one C1 peak as shown in Figure 2a indicated that DMPC molecules were moving rapidly to such an extent that the two signals became a motionally averaged peak. The C1 chemical shift value of the  $^{13}\text{C}$  CP-MAS spectra at  $n_W = 11$  is 173.3 ppm (Figure 2a). It is almost an average value of the two C1 chemical shift values for isomer I of crystalline DMPC at  $n_W = 4$  (175.4 and 171.8 ppm (Figure 2c)). Mei et al. demonstrated that a structure similar to isomer B of the DMPC crystal structure<sup>27</sup> is the predominant conformation in the liquid-crystalline DMPC bilayer. These reasons led us to suspect that the head groups of DMPC at  $n_W \geq 9$  are moving rapidly.



Additionally, isomer I of the crystalline state at  $n_W = 4$  takes the same conformation of the DMPC molecule at  $n_W \geq 9$ . On the other hand, the acyl chains in DMPC molecules adopted almost an all-trans conformation in the crystalline state at  $n_W = 4$  and a trans-gauche conformation at  $n_W \geq 9$  (Figure 2).

In the current study, the use of a higher-field magnet (600 MHz) than that used in the Bruzik and Harwood study (300 MHz) helped us to acquire spectra of crystalline DMPC with a higher resolution. We successfully assigned the  $^1\text{H}$  and  $^{13}\text{C}$  NMR spectra of the crystalline DMPC at  $n_W = 4$  containing two isomers. As mentioned above, the  $^{13}\text{C}$  NMR spectrum of the DMPC crystal<sup>40</sup> exhibited a modest difference from that in this study (Figure 2c). For example, both spectra have four C1 peaks. As shown in Table 1, the C1 peaks were assigned as 175.4 ppm (*sn*-2, conformation B), 173.8 ppm (*sn*-1, conformation A), 171.8 ppm (*sn*-1, conformation B), and 170.6 ppm (*sn*-2, conformation A) in this study. For the DMPC crystal reported by Bruzik and Harwood, the C1 peaks appeared at 175.0, 173.9, 173.2, and 171.4 ppm. The peak at 170.6 ppm (*sn*-2, conformation A in this study) shown in Figure 2c was the only one that had a different chemical shift value among the four C1 peaks. This indicates that the *sn*-2 C1 carbon in conformation A takes a different conformation from the DMPC crystal made by Bruzik and Harwood. They also reported chemical shift values as follows: C $\alpha$  (61.0, 60.1 ppm), G2 (74.2, 69.7 ppm), and G3 (62.8, 61.45 ppm). Comparing these values to our assigned values shown in Table 1, the chemical shift values of C $\alpha$  are almost the same, but those of G2 and G3 are different. Therefore, we surmise that not only the *sn*-2 C1 carbon in conformation A but also the structures around glycerol backbone moiety used in this study are different from their crystal structure. This structural difference might result from the water/lipid ratio,  $n_W$ . The DMPC crystal, used in the X-ray<sup>27</sup> and NMR<sup>40</sup> studies, contained two water molecules per one DMPC molecule, whereas in this study, DMPC forms a crystalline state at  $n_W = 4$ . The difference in the hydrogen bonding network probably brings about the difference in the conformation of glycerol and the *sn*-2 C1 carbon moiety in the DMPC molecules.

Since  $^{13}\text{C}$  chemical shift values are really sensitive to backbone geometry, quantum chemical calculations for  $^{13}\text{C}$  chemical shift values have been used to predict and assess molecular structures from small molecules to large proteins.<sup>41,42</sup> A comparison between the assigned chemical shift values from solid-state NMR and calculated values for the X-ray crystal structures of DMPC (Figure 7) shows good agreement between isomer I and B and isomer II and A, respectively. In addition, all calculated values were deshielded. In particular, C $\beta$  and C1 carbons in both isomers show large downfield shifts of about 10 ppm in calculated values. Generally, the density functional calculation of nuclear shielding deviates from experimental values downfield.<sup>43–45</sup> This is commonly due to the overestimation of magnitude of the paramagnetic contribution with common density functionals. Mulder and Filatov have reported that deviations from experimental values of the  $^{13}\text{C}$  chemical shifts calculated with DFT methods at the GIAO-B3LYP are all to downfield about 1–4 ppm for a carbon with single bond; however, they are about 10–15 ppm for a carbon with multiple bonds and bonded to a heteroatom.<sup>45</sup> For this reason, the large downfield shift of C1 is reasonable; however, the deviations of the C $\beta$  carbons are a little large. The large deviations of C $\beta$  appeared to result from the structural difference between the X-ray crystalline structure and the crystalline DMPC structure examined in this study. Aside

from this, the good agreement between the assigned chemical shift values in the present study and the calculated values for the X-ray crystalline structure indicates that we can prepare equal quality DMPC crystals without recrystallization from a mixture of organic solvents.

A few studies have previously reported the assignment of the NMR signal of the crystal as having more than one inequivalent molecular conformation in a unit cell. Here, the number of conformations in a unit cell is denoted by the symbol  $Z$ . Olsen et al. assigned the vitamin-D<sub>3</sub> ( $Z = 2$ ) signal using the through-bond  $^{13}\text{C}$ – $^{13}\text{C}$  correlation spectrum (UC2QF COSY) of the natural abundance sample.<sup>46</sup> They produced a well-resolved 2D NMR spectrum and completely assigned it. This method is really useful but not applicable to the assessment of the natural abundance sample of the crystalline DMPC at  $n_W = 4$ . This is because the signal-to-noise ratio is not high enough to obtain the 2D spectrum unless we use uniformly  $^{13}\text{C}$ -labeled DMPC. Harper et al. have reported the signal assignment in santonin ( $Z = 2$ ), phase I and II of calcium acetate ( $Z = 2$ , with four independent acetates), and catechin ( $Z = 2$ ) solely using HETCOR.<sup>47</sup> Due to low  $^1\text{H}$  resolution, complete assignment of all separate molecules of the asymmetric unit in santonin and phase I of calcium acetate was difficult, whereas complete assignment was achieved in phase II of calcium acetate and catechin because of having sufficient  $^1\text{H}$  resolution. In this study, complete assignment would have been difficult if we had used only HETCOR experiments due to low  $^1\text{H}$  resolution. However, the combined use of MAS-J-HMQC and HETCOR (Figure 4) with two kinds of DARR (Figures 5 and 6) experiments allowed us to overcome these difficulties to accomplish the almost complete resonance assignment.

The  $^{13}\text{C}$  NMR spectrum of the OTS-coated glass aligned DMPC bilayers shown in Figure 8c had almost the same spectral pattern as that of the crystalline DMPC at  $n_W = 4$  (Figure 2c, 3c, and 3d). This proved that we can also obtain highly ordered, crystalline DMPC simply by drying the sample from DMPC MLV dispersions (without mixing). A comparison of sample dehydration on a non-OTS-coated glass slide and an OTS-coated glass slide (Figure 8d and 8c) showed that OTS coating has a strong effect on molecular ordering. This is probably for the following two reasons: (i) The difference of the wettability of the glass surfaces. When DMPC MLV dispersions were deposited on the surfaces of the glass slides, their fluid was more wettable on the non-OTS-coated glass surfaces than on the OTS-coated glass surfaces. Due to the limited spreading of the liquid on the OTS-coated glass surface, the dehydration process probably progressed more slowly. This slow dehydration process enabled DMPC molecules to have two kinds of low energy conformations (isomers I and II) and form the crystalline phase. (ii) The difference of affinity between the phospholipids and the glass surfaces. On a non-OTS-coated glass slide, phospholipids are known to align on the slide with their head groups down, because the surface of the glass is hydrophilic.<sup>48</sup> On the other hand, on an OTS-coated glass slide, phospholipids are known to align on the slide with their acyl chains down.<sup>49</sup> Compared with the interaction between a non-OTS-coated glass slide and phospholipid head groups, the interaction between an OTS-coated glass slide and phospholipid acyl chains is stronger because of the energetic gain from the hydrophobic interactions. This gives the OTS coating a stronger driving force for the self-assembly of phospholipids on the glass surface.

In this study, we did not try to make crystalline DMPC sample in the presence of buffer solution because ions in buffer solution

will become highly concentrated after drying the sample. We think it is possible to make a crystalline membrane with appropriate buffer concentration. The presence of ions in the buffer solution would bring about different molecular packing and different spectral patterns, and it will reproduce more physiological conditions. However, it is difficult to make a consistent buffer concentration at each water/lipid ratio. Since one of the aims of this study is to examine the temperature and hydration level dependence of DMPC, we consistently prepared the samples without ions.

To date, mechanically glass-aligned samples of membrane have been prepared to examine the mobility and orientation of the membrane itself<sup>10,11,49</sup> and the proteins and peptides in membranes.<sup>12,13</sup> Usually, samples are distributed over the surface of a glass plate, and then about 20–30 glass plates are stacked. After hydration levels are optimized, the glass-aligned samples are placed in the radio frequency coil in a flat-coil probe<sup>50</sup> or NMR tube. Next, the NMR spectra are measured under static conditions. The resulting information is an orientation of the specific site of the molecules with respect to the membrane normal. In our case, the dehydrated surface-ordered sample on an OTS-coated glass slide is separated from the glass plate. After cutting it into small pieces, samples are transferred to an NMR tube. This can be regarded as a microcrystalline sample. The sample is measured by NMR with a normal NMR probe under MAS. Consequently, the information on the relative orientation of the membrane to a static field is not obtainable. However, since the sample is in a crystalline state, we can avoid the unwanted broadening arising from conformational distribution. Therefore, if we can extend this novel sample preparation method to the membrane containing protein or peptide, it should be a powerful method because we can obtain a high-resolution protein spectrum. Marrasi and Kevin have reported that they prepared glass oriented lipid bilayer samples containing protein with a single pair of glass slides and then measured the sample with glass slides in a flat-coil probe.<sup>51</sup> They demonstrated that the spectral features of the uniformly <sup>15</sup>N-labeled membrane protein CHIF (channel inducing factor) in a hydrated DMPC bilayer at a hydration level of  $n_W = 4$  are not different from the spectral features at  $n_W = 10$ . They also pointed out that the resonances of CHIF show the same orientation of protein in both samples. Therefore, we may expect that the conformation of the protein in the membrane is not significantly affected by the hydration levels in the range of  $n_W = 4$ –10. Accordingly, if we reconstruct membrane proteins/peptides into a lipid bilayer and crystallize it using our proposed methods, we should have a higher chance of obtaining cocrystals of membrane proteins/peptides and lipids. Of note is that there is an advantage to the crystalline sample, in addition to eliminating the line broadening. Namely, we can recouple the anisotropic interaction without scaling down, owing to sufficient suppression of molecular motion by sample dehydration. This method is beneficial to determine intermolecular interactions that are usually difficult to examine, particularly in cases where molecular motions are sufficiently maintained under hydrated or liquid crystalline conditions. Assuming that we can prepare crystalline membrane-associated protein samples with the current method, this method deserves further investigation to determine the high precision structures of membrane-associated protein and to detect membrane–protein or ligand–receptor protein interactions.

## V. CONCLUSIONS

We showed high-resolution <sup>13</sup>C CP-MAS NMR spectra of a highly ordered crystalline DMPC sample with a defined hydration under MAS. We prepared the crystalline DMPC in two ways: (i) by drying DMPC MLV dispersions under a nitrogen stream and mixing thoroughly with a spatula on a glass plate or (ii) by simply dehydrating them on an OTS-coated glass slide. Crystalline DMPC prepared by these two methods showed the same spectral pattern, indicating that DMPC molecules in both samples are most likely in their equilibrium state. The fact that the number of peaks doubled suggests that molecules take two different conformations in the crystal. Using solid-state NMR methods, the <sup>1</sup>H and <sup>13</sup>C NMR spectra of the crystalline DMPC containing two isomers were completely assigned, which provided us with basic information for further solid-state NMR studies related to (micro)crystalline membranes. A comparison between experimental and calculated chemical shift values confirmed that the two isomers in the crystalline DMPC took almost the same conformations as those found in X-ray crystal structures of DMPC.<sup>27</sup> Thus, the crystalline DMPC examined in the present study was shown to be of equal quality with DMPC crystals, which were prepared by recrystallization from a mixture of organic solvents in the X-ray study. The fact that we could obtain a high-quality crystalline membrane by methods (i) and (ii) points to the importance of homogeneous drying, as well as the self-assembly of molecules (through the orientation of DMPC under the assistance of the OTS surface), both of which take place during the drying process. Refinement and development of methodology deserve further investigation to establish how to acquire ideal crystalline macromolecular membrane complexes for X-ray crystallography or NMR analyses.

## AUTHOR INFORMATION

### Corresponding Author

\*Tel.: +81-75-962-6152. Fax: +81-75-962-2115. E-mail: nomura@sunbor.or.jp.

## ACKNOWLEDGMENT

We thank Ms. Saori Mori (NAIST, Osaka, Japan) for her assistance in the preparation of glass slides. We also thank Dr. Takashi Iwashita for many scientific discussions. Further, we would like to thank Dr. Makoto Suematsu for his valuable comments. This work was supported by a Grant-in-Aid for Scientific Research (#19550174) to K.N. from the Ministry of Education, Culture, Sports, Science and Technology of Japan. The authors also thank Suntory Holdings for their financial support.

## REFERENCES

- (1) Andrew, E. R.; Bradbury, A.; Eades, R. G. *Nature* **1958**, *182*, 1659.
- (2) Lowe, I. J. *Phys. Rev. Lett.* **1959**, *2*, 285–287.
- (3) Gross, J. D.; Warschawski, D. E.; Griffin, R. G. *J. Am. Chem. Soc.* **1997**, *119*, 796–802.
- (4) Saito, H. *Magn. Reson. Chem.* **1986**, *24*, 835–852.
- (5) Castellani, F.; van Rossum, B.; Diehl, A.; Schuber, M.; Rehbein, K.; Oschkinat, H. *Nature* **2002**, *420*, 98–102.
- (6) Franks, W. T.; Zhou, D. H.; Wylie, B. J.; Money, B. G.; Graesser, D. T.; Frericks, H. L.; Sahota, G.; M., R. C. *J. Am. Chem. Soc.* **2005**, *127*, 12291–12305.

- (7) McDermott, A.; Polenova, T.; Bockmann, A.; Zilm, K. W.; Paulsen, E. K.; Martin, R. W.; Montelione, G. T. *J. Biomol. NMR* **2000**, *16*, 209–219.
- (8) Zech, S. G.; Wand, A. J.; McDermott, A. E. *J. Am. Chem. Soc.* **2005**, *127*, 8618–8626.
- (9) Pope, J. M.; Cornell, B. A. *Chem. Phys. Lipids* **1979**, *24*, 27–43.
- (10) Braach-Maksvytis, V. L. B.; Cornell, B. A. *Biophys. J.* **1988**, *53*, 839–843.
- (11) Cornell, B. A.; Separovic, F.; Braldassi, A.; Smith, R. *Biophys. J.* **1988**, *53*, 67–76.
- (12) Cross, T. A.; Opella, S. J. *Curr. Opin. Struct. Biol.* **1994**, *4*, 574–581.
- (13) Opella, S. J.; Marassi, F. M.; Gesell, J. J.; Valente, A. P.; Kim, Y.; Montal, M. O.; Montal, M. *Nat. Struct. Biol.* **1999**, *6*, 374–379.
- (14) Glaubitz, C.; Watts, A. *J. Magn. Reson.* **1998**, *130*, 305–316.
- (15) Mason, A. J.; Grage, S. L.; Straus, S. K.; Glaubitz, C.; Watts, A. *Biophys. J.* **2004**, *86*, 1610–1617.
- (16) Sizun, C.; Bechinger, B. *J. Am. Chem. Soc.* **2002**, *124*, 1146–1147.
- (17) Fung, B. M.; Khitrin, A. K.; Ermolaev, K. *J. Magn. Reson.* **2000**, *142*, 97–101.
- (18) Lesage, A.; Charmont, P.; Steuernagel, S.; Emsley, L. *J. Am. Chem. Soc.* **2000**, *122*, 9739–9744.
- (19) Lesage, A.; Emsley, L. *J. Magn. Reson.* **2001**, *148*, 449–454.
- (20) Bielecki, A.; Kolbert, A. C.; Levitt, M. H. *Chem. Phys. Lett.* **1989**, *155*, 341–346.
- (21) van Rossum, B. J.; Foerster, H.; deGroot, H. J. M. *J. Magn. Reson.* **2003**, *124*, 516–519.
- (22) Takegoshi, K.; Nakamura, S.; Terao, T. *Chem. Phys. Lett.* **2001**, *344*, 631–637.
- (23) Takegoshi, K.; Nakamura, S.; Terao, T. *J. Chem. Phys.* **2003**, *118*, 2325–2341.
- (24) Takegoshi, K.; Terao, T. *J. Chem. Phys.* **2002**, *117*, 1700–1707.
- (25) Morcombe, C. R.; Zilm, K. W. *J. Magn. Reson.* **2003**, *162*, 479–486.
- (26) Dvinskikh, S. V.; Castro, V.; Sandstrom, D. *Magn. Reson. Chem.* **2004**, *42*, 875–881.
- (27) Pearson, R. H.; Pascher, I. *Nature* **1979**, *281*, 499–501.
- (28) Frisch, M. J.; Trucks, G. W.; Schlegel, H. B.; Scuseria, G. E.; Robb, M. A.; Cheeseman, J. R.; Montgomery, J. A.; Vreven, T.; Kudin, K. N.; Burant, J. C.; Millam, J. M.; Iyengar, S. S.; Tomasi, J.; Barone, V.; Mennucci, B.; Cossi, M.; Scalmani, G.; Rega, N.; Petersson, G. A.; Nakatsuji, H.; Hada, M.; Ehara, M.; Toyota, K.; Fukuda, R.; Hasegawa, J.; Ishida, M.; Nakajima, T.; Honda, Y.; Kitao, O.; Nakai, H.; Klene, M.; Li, X.; Knox, J. E.; Hratchian, H. P.; Cross, J. B.; Bakken, V.; Adamo, C.; Jaramillo, J.; Gomperts, R.; Stratmann, R. E.; Yazyev, O.; Austin, A. J. C.; R.; Pomelli, C.; Ochterski, J. W.; Ayala, P. Y.; Morokuma, K.; Voth, G. A.; Salvador, P.; Dannenberg, J. J.; Zakrzewski, V. G.; Dapprich, S.; Daniels, A. D.; Strain, M. C.; Farkas, O.; Malick, D. K.; Rabuck, A. D.; Raghavachari, K.; Foresman, J. B.; Ortiz, J. V.; Cui, Q.; Baboul, A. G.; Clifford, S.; Cioslowski, J.; Stefanov, B. B.; Liu, G.; Liashenko, A.; Piskorz, P.; Komaromi, I.; Martin, R. L.; Fox, D. J.; Keith, T.; Al-Laham, M. A.; Peng, C. Y.; Nanayakkara, A.; Challacombe, M.; Gill, P. M. W.; Johnson, B.; Chen, W.; Wong, M. W.; Gonzalez, C.; Pople, J. A. *Gaussian 03*, Revision C.02; Gaussian, Inc.: Wallingford, CT, 2004.
- (29) Hong, M.; Schmidt-Rohr, K.; Zimmermann, H. *Biochemistry* **1996**, *35*, 8335–8341.
- (30) Sanders, C. R. *Biophys. J.* **1993**, *64*, 171–181.
- (31) Bechinger, B.; Seelig, J. *Chem. Phys. Lipids* **1991**, *58*, 1–5.
- (32) Cevc, G.; Marsh, D. *Biophys. J.* **1985**, *47*, 21–23.
- (33) Faure, C.; Bonakdar, L.; Dufourc, E. J. *FEBS Lett.* **1997**, *405*, 263–266.
- (34) Ulrich, A. S.; Watts, A. *Biophys. J.* **1994**, *66*, 1441–1449.
- (35) Rummey, J. M.; Boyce, M. C. *J. Chem. Educ.* **2004**, *81*, 762–763.
- (36) Janiak, M. J.; Small, D. M.; Shipley, G. G. *J. Biol. Chem.* **1979**, *254*, 6068–6078.
- (37) Dubois, L. H.; Nuzzo, R. G. *Annu. Rev. Phys. Chem.* **1992**, *43*, 437–467.
- (38) Swalen, J. D.; Allara, D. L.; Andrade, J. D.; Chandross, E. A.; Garoff, S.; Israelachvili, J.; McCarthy, T. J.; Murray, R.; Pease, R. F.; Rabolt, J. F.; Wynne, K. J.; Yu, H. *Langmuir* **1987**, *3*, 932–950.
- (39) Plant, A. L. *Langmuir* **1999**, *15*, 5128–5135.
- (40) Bruzik, K. S.; Harwood, J. S. *J. Am. Chem. Soc.* **1997**, *119*, 6629–6637.
- (41) Cornilescu, G.; Delaglio, F.; Bax, A. *J. Biomol. NMR* **1999**, *13*, 289–302.
- (42) Neal, S.; Nip, A. M.; Zhang, H.; Wishart, D. S. *J. Biomol. NMR* **2003**, *26*, 215–240.
- (43) Bagno, A.; Rastrelli, F.; Saielli, G. *J. Phys. Chem. A* **2003**, *107*, 9964–9973.
- (44) Cheeseman, J. R.; Trucks, G. W.; Keith, T. A.; Frisch, M. J. *J. Chem. Phys.* **1996**, *104*, 5497–5509.
- (45) Mulder, F. A. A.; Filatov, M. *Chem. Soc. Rev.* **2009**, *39*, 578–590.
- (46) Olsen, R. A.; Struppe, J.; Elliott, D. W.; Thomas, R. J.; Mueller, L. J. *J. Am. Chem. Soc.* **2003**, *125*, 11784–11785.
- (47) Harper, J. K.; Strohmeier, M.; Grant, D. M. *J. Magn. Reson.* **2007**, *189*, 20–31.
- (48) Richter, R. P.; Berat, R.; Brisson, A. R. *Langmuir* **2006**, *22*, 3497–3505.
- (49) Separovic, F.; Cornell, B.; Pace, R. *Chem. Phys. Lipids* **2000**, *107*, 159–167.
- (50) Bechinger, B.; Opella, S. J. *J. Magn. Reson.* **1991**, *95*, 585–588.
- (51) Marassi, F. M.; Crowell, K. C. *J. Magn. Reson.* **2003**, *161*, 64–69.